Molecular basis for PICS-mediated piRNA biogenesis and cell division

Xiaoyang Wang[1,#], Chenming Zeng[1,#], Shanhui Liao[1,#], Zhongliang Zhu[1], Jiahai Zhang[1], Xiaoming Tu[1], Xuezhu Feng[1,*], Shouhong Guang[1,*], and Chao Xu[1,*]

[1] Ministry of Education Key Laboratory for Membraneless Organelles & Cellular Dynamics, Hefei National Laboratory for Physical Sciences at the Microscale, School of Life Sciences, Division of Life Sciences and Medicine, University of Science and Technology of China, 230027, Hefei, P.R. China

[#]These authors contributed equally: Xiaoyang Wang, Chenming Zeng, and Shanhui Liao

*To whom correspondence should be addressed. E-mail: fengxz@ustc.edu.cn; sguang@ustc.edu.cn; xuchaor@ustc.edu.cn

Running title: Structural insights into PICS complex

Keywords: piRNA biogenesis, chromosome segragation, PICS complex, perinuclear granule

Abstract

By incorporating two mutually exclusive factors, PID-1 and TOST-1, *C. elegans* PICS complex plays important roles in piRNA biogenesis, chromosome segregation and cell division, respectively. We firstly mapped the interaction network between PICS subunits. By solving the several complex structures, including those of TOFU-6/PICS-1, ERH-2/PICS-1, and ERH-2/TOST-1, we uncover the mechanisms underlying the interactions between PICS subunits. Our biochemical experiment demonstrates that PICS exists as an octamer consisting of two copies of each subunits. Combining structural analyses with mutagenesis experiments, we identified residues of PICS subunits that are critical for maintaining intact PICS complex *in vitro*. Furthermore, using genetics, cell biology and imaging experiments, we found that those mutants impairing the *in vitro* interaction network within PICS, also lead to abnormal dysfunction PICS *in vivo*, including mislocalization of PICS, and reduced levels of piRNAs or abnormal chromosome segregation and cell division. Therefore, our work provides structural insights into understanding the PICS-mediated piRNA biogenesis and cell division.

Introduction

PIWI-interacting RNAs (piRNA) associate with Piwi family proteins, and paly essential roles in transposon silencing and gene regulation [1, 2, 3, 4, 5]. Piwi proteins were firstly discovered as essential factors for stem cell self-renewal in *Drosophila* [6]. Lack of piwi proteins also leads to male sterile in mice and human [7, 8, 9, 10]. In *C. elegans*, piRNAs are bound by Piwi protein PRG-1 and recognize target sequences that depends on a mismatch-tolerant rule between piRNA sequences and their targets [11, 12, 13, 14, 15, 16, 17, 18]. Upon targeting, the piRNA/PRG-1 complex recruits RNA-dependent RNA polymerase to drive the biogenesis of secondary small interfering RNA to conduct the silencing of piRNA targets [4, 19, 20, 21, 22, 23, 24].

Diverged piRNA biogenesis pathways exist in animals [3]. In the germline of *C. elegans*, piRNA precursors are mainly transcribed by RNA polymerase II from thousands of piRNA loci containing a core DNA consensus motif, which is termed as "Ruby motif" [25, 26]. The upstream sequence transcription complex (USTC), containing PRDE-1, SNPC-4 and TOFU-4/5, initiates the transcription of piRNA genes, while the integrator complex and the RNA polymerase II subunit RBP-9 act in the termination of piRNA transcription [27, 28, 29, 30, 31, 32]. SNPC-1.3 associates with SNPC-4 and promotes the piRNA transcription in males [33]. After transcription, the precursors are transported into cytoplasm or perinuclear granules and are decapped to remove two nucleotides at 5' ends, allowing them to be loaded by PRG-1 [3, 19, 20, 21]. For the PRG-1-bound piRNA, its extra nucleic acids at 3' ends are trimmed by the exonuclease, PARN-1 [34]. At the final step of piRNA maturation, the 2'-O-methylation at 3' termini is carried out by HENN-1 [35, 36, 37]. The mature piRNAs have a precise length of 21 nt, starting with a 5' monophosphorylated uracil and ending with a 2'-O-methylated 3' residue, thereby termed as 21U-RNAs [19, 20, 25].

By using functional proteomics, we and another group independently identified a piRNA biogenesis and chromosome segregation (PICS) complex (also named as PETISCO) that plays important roles in 21U-RNA biogenesis, chromosome segregation and cell division [38, 39]. The PICS-1 complex is composed of TOFU-6, PICS- 1 (also names as PID-3), ERH-2 and two mutually exclusive factors, PID-1 and

TOST-1. The PID-1 containing complex is functional in piRNA maturation and processes piRNA precursors at 5' termini via its association with the *C. elegans* elF4E ortholog IFE-3, while the TOST-1 containing form is essential for chromosome segregation and cell division in embryos, suggesting that a potential crosstalk exists between the two biological events [38, 39, 40, 41]. However, how PICS subunits interact with each other and how PID-1 and TOST-1 mutually exclude each other, are largely unknown.

To provide structural insights into the PICS complex, we first examined the interactions between PICS subunits by using the Isothermal Titration Calorimetry (ITC) binding assay. ITC binding data indicate that the RRM domain and a fragment upstream of the RRM domain of PICS-1 interact with the TOFU-6 RRM domain and ERH-2, respectively, and TOST-1 and PID-1 bind to ERH-2 in a mutually exclusive manner. Then we solved the complex structure of PICS-1^{RRM} with TOFU-6^{RRM}, in which the PICS-1^{RRM} homodimer binds two TOFU-6^{RRM} molecules to form a heterotetramer. Next we solved the structures of ERH-2 homodimer bound with either a PICS-1 fragment or a TOST-1 fragment, and found that PICS-1 and TOST-1 binds to different surfaces of ERH-2, whereas PID-1 and TOST-1 bind to ERH-2 in a competitive manner. Our structures support that PICS complex is an octamer formed by two copies of each four subunits. In PICS, one ERH dimer binds to one TOFU-6^{RRM}/PICS-1^{RRM} heterotetramer to form a hexamer, and two copies of TOST-1 or PID-1 further bind to the hexamer to form the octamer. We validated the binding interface between PICS subunits by using mutagenesis and ITC binding experiments. Furthermore, we found that the disruption of PICS complex *in vivo* leads to reduced amount of mature piRNAs or the delay in chromosome segregation during cell division. Overall our structure research, complemented by *in vitro* biochemistry and *in vivo* cell biology experiments, not only unveils the molecular mechanism underlying PICS formation, but also sheds light on the role of PICS complex in piRNA maturation and chromosome segregation.

Results

Interaction network within PICS mapped by ITC binding assay

Previously, we and another group identified the PICS complex and mapped the protein-protein interactions (PPIs) by pull-down and western blot experiments (**Fig. 1a**) [38, 39]. Here we cloned, expressed, and purified the RRM domains of TOFU-6 (TOFU-6^{RRM}, residues 2-92) and PICS-1 (PICS-1^{RRM}, residues 201-282), respectively, and examined their binding affinity by ITC. The ITC binding data indicate that the TOFU-6^{RRM} binds to PICS-1^{RRM} with a K_d of 6.2 nM **(Fig. 1b, Supplementary Table 1**). By ITC binding assay, we found that ERH-2 binds to a region upstream of PICS-1^{RRM} (residues 180-200), named as ERH-2 binding motif (EBM) thereafter, with a K_d of 8.5 μM. In addition, ERH-2 also binds to two fragments derived from PID-1 (PID-1$^{50-70}$) and TOST-1 (TOST-1$^{34-54}$) with K_ds of 18 μM and 3.2 μM, respectively (**Supplementary Table 1**). To increase the solubility of above ERH-2 binding fragments, we fused them to the C-terminus of SUMO protein and the K_ds are for the binding between ERH-2 and SUMO fusion proteins. As a negative control, SUMO protein itself displays no binding affinity towards ERH-2 (**Supplementary Table 1**).

To understand how ERH-2 bind to different ligands *in vitro* simultaneously, we fused ERH-2 with PICS-1$^{180-200}$ and TOST-1$^{34-54}$ via a 21-aa linker ((Gly-Ser-Ser)$_7$) and an 18-aa linker ((Gly-Ser-Ser)$_6$), respectively. We then examined the binding of PID-1$^{50-70}$ to the two fusion proteins to study the ERH-2/PID-1 interaction in the presence of PICS-1 or TOST-1. ITC binding data indicate that PID-1 binds to ERH-2-(GSS)$_7$-PICS-1 but not ERH-2-(GSS)$_6$-TOST-1, with a comparable binding affinity with ERH-2 only (12 μM vs. 18 μM) (**Supplementary Table 1**), suggesting that TOST-1 but not PICS-1 interferes with the *in vitro* interaction between ERH-2 and PID-1. Taken together, the ITC binding experiments suggest that both PICS-1 and ERH-2 serve as scaffold molecules to tether different factors within PICS complex.

Crystal structure of PICS-1^{RRM}-TOFU-6^{RRM} tetramer

To understand how PICS-1^{RRM} interacts with TOFU-6^{RRM}, we crystalized the complex and solved the SeMet and native structures at resolutions of 1.95 Å and 2.68 Å, respectively (**Supplementary Table 2**). Given that the two structures are almost

identical, the native one was used for structural analysis. In the complex, the two PICS-1^{RRM} molecules (PICS-1^{A} and PICS-1^{B}) a symmetric homodimer homodimer (P2), with each of them adopting canonical RRM fold (β1-α1-β2-β3-α2-β4) (**Fig. 1c, Supplementary Fig. 1a-1b**) [42]. Two molecules of TOFU-6^{RRM} (TOFU-6^{C} and TOFU-6^{D}) contact P2 from in a symmetric manner, with each TOFU-6^{RRM} interacts with both protomers of P2 to form the TOFU-6/PICS-1 tetramer (T2-P2) (**Fig. 1c**).

The two PICS-1^{RRM} interact with each other through α1, β2, and the linker connecting α1 and β2, with α1^{A} nearly perpendicular to α1^{B} (**Fig. 1d-1e**). For one half of the interface, Phe217^{A} is buried in a hydrophobic pocket composed of Phe217^{B}, Ala220^{B}, V228^{B}, and I231^{B} (**Fig. 1e**). In addition, several hydrogen bonds are formed, including one between main chain carboxyl group of Met213^{A}, and one between the side chain of Asn215^{A} and the main chain carboxyl group of Val228^{B}, and two between the side chain amide group of Gln221^{A} and the main chain carboxyl groups of Ala220^{B} and Tyr226^{B} (**Fig. 1e**). Altogether, both hydrophobic and electrostatic interactions contribute to the dimerization and the other half of the dimerization interface could be obtained via the symmetry.

TOFU-6^{RRM} is longer than PICS-1^{RRM}, and it contains five anti-parallel β-strands with β4 as the additional one immediately after α2 (**Supplementary Fig. 2a-2b**). TOFU-6^{C} primarily interacts with PICS-1^{A} through α1-β2 of TOFU-6^{C}, and α2 and a C-terminal fragment of PICS-1^{A} (**Fig. 2a-2c**). α1 of TOFU-6^{C} interacts with α2 of PICS-1^{A} via both hydrophobic and electrostatic interactions (**Fig. 2b**). Specifically, Trp27, Phe30, His31, and Cys42 of TOFU-6^{C}, make hydrophobic interactions with Lys246, Phe247, and Tyr250 of PICS-1^{A}. Asp26 and Gln34 of TOFU-6^{C} form salt bridges with Lys246 and Gln254 of PICS-1^{A}, respectively (**Fig. 2b**). In addition, α1 of TOFU-6^{C} also interacts with the PICS-1 C-terminus via electrostatic interactions (**Fig. 2b**). The imidazole ring of TOFU-6^{C} His31 hydrogen bonds to the side chain of the PICS-1^{A} Ser275; the TOFU-6^{C} Asn25 forms two hydrogen bonds via its side chain with the main chain groups of Ser276 and Ala278 of PICS-1^{A}; the side chain of Asn28 also forms two hydrogen bonds with the main chain groups of Ala278 and Val279 of PICS-1^{A} (**Fig. 2b**). Two loops of TOFU-6^{C}, one between α1 and β2 and the other

between β3 and α2, also interacts with PICS-1^{A} (**Fig. 2c**). Lys38 and Met61 of Tofu-6^{C} make hydrophobic contacts with Pro225 and Tyr226 of PICS1^{A}; TOFU-6^{C} Val39 forms two main chain hydrogen bonds with the side chain of PICS-1^{A} Gln251, and TOFU-6^{C} Ser40 also forms two hydrogen bonds via its main chain carboxyl group with the side chain amide groups of Asn245 and Gln248 (**Fig. 2c**).

TOFU-6^{C} also contacts with the other protomer of PICS-1 (PICS-1^{B}) (**Fig. 2d**). The N-terminus and α2 of TOFU-6^{C} interact with two loops of PICS-1^{B}, one between β1 and α1 and the other between α2 and β4. Tyr8 and Leu10 of TOFU-6^{C} make hydrophobic contacts with Pro211, Met213, and His265 of PICS-1^{B}. Asp12 and Asp67 of TOFU-6^{C} form salt bridges with Arg263 of PICS-1^{B}. Due to symmetry, TOFU-6^{D} also interacts with both protomers of P2, primarily via PICS-1^{B} (**Fig. 1c**).

To validate the P2 interface that constitutes the basis of the heterotetramer, we chose to mutate Phe217 of PICS-1^{RRM} to Glu and found by gel filtration chromatography that F217E disrupts the PICS-1^{RRM} homodimer by introducing repulsive charges and potential steric clashes (**Supplementary Fig. 3a**), confirming the key role of Phe217 in the P2 dimer interface. Also, the PICS-1^{RRM} F217E reduced the TOFU-6^{RRM} binding affinity by ~90-fold (K_ds: 6.2 nM vs. 570 nM) (**Supplementary Fig. 3b, Supplementary Table 1**), suggesting that the second interface between P2 and TOFU-6^{RRM} is important for maintaining high binding affinity within the tetramer. Next we chose to mutant residues at the PICS-1^{RRM}/TOFU-6^{RRM} interface and examined their effect by ITC binding assays. ITC data indicate all mutants, including Y250A/Q251A and K246A/F247A of PICS-1^{RRM}, and D26A/W27A of TOFU-6 ^{RRM}, reduced the binding affinity by ~2700-4500 folds (K_ds: 6.2 nM vs. 17-30 μM) (**Fig. 2e-2g, Supplementary Table 1**), further validating the PICS-1^{RRM}/TOFU-6^{RRM} interface. Collectively, our mutagenesis experiments and ITC binding data confirmed the roles of residues at P2 dimer and T2-P2 tetramer interfaces, demonstrating that an intact P2 is required for binding to TOFU-6^{RRM} with high affinity.

Structure of ERH-2 bound to PICS-1^{EBM}

Our ITC data showed that ERH-2 binds to PICS-1^{EBM} (**Fig. 3a**). To uncover the molecular mechanism underlying ERH-2/PICS-1 interaction, we tried the co-crystallization of ERH-2 with the EBM of PICS-1, but failed to get any diffractable crystal. Then we fused a fragment of ERH-2 (1-103) with the EBM of PICS-1 (180-200) via a $(GSS)_7$ linker, crystallized the fusion protein, and solved its structure at a resolution of 2.40 Å (**Supplementary Table 2**). The overall structure is a tetramer formed by ERH-2 and PICS-1^{EBM} in a 2:2 ratio. In the structure, the ERH-2 homodimer adopts a butterfly-like architecture with the antiparallel β sheet from each protomer packed against each other (**Fig. 3b**). The structure of *C. elegans* ERH-2 is similar to its human and yeast orthologs with the root-mean-square deviations (RMSDs) in a range of 1.1-1.3 Å (**Supplementary Fig. 4**).

Two PICS-1^{EBM} molecules, named as EBM^C and EBM^D, respectively, are visible in the structure with each of them adopting a helix structure (**Fig. 3b**). The EBM^C is accommodated into a v-shape concave via contacting with both ERH-2 molecules, ERH-2^A and ERH-2^B, respectively (**Fig. 3b**). EBM^C mainly interacts with the β1, β2, α1, and α2 of ERH-2^A, and extensive hydrophobic interactions are found throughout their binding interface. EBM^C also interacts with the η1 of ERH-2^B via its C-terminus (**Fig. 3c**). On one side, I182, V186, Phe187, and Leu190 of EBM^C make hydrophobic interactions with Ile11, Thr13, Met38, Phe42, Phe61, and Leu65 of ERH-2^A; on the other side, Val189 of EBM^C is accommodated into a hydrophobic pocket composed of Ala34, Lys37, and Met38 of ERH-2^A (**Fig. 3c**). In addition to hydrophobic interactions, the main chain of EBM^C Asp181 and the side chain of EBM^C Ser185 are hydrogen bonded to the side chain of Lys45^A; the side chain of EBM^C Ser185 forms another hydrogen bond with ERH-2^A Asp41; the main chain of EBM^C Leu190 is hydrogen bonded to the side chain of ERH-2^B Arg20 and the side chain of EBM^C His191 form two hydrogen bonds with the side chains of ERH-2^A Thr21 and ERH-2^B Arg20, respectively. EBM^C His191 also makes hydrophobic interaction with Leu17^B (**Fig. 3c**). EBM^D contacts with the ERH-2 dimer in a symmetrical manner (**Fig. 3b**). Taken together, each PICS-1^{EBM} contacts with both protomers of ERH-2 dimer through both hydrophobic and hydrogen bonding interactions.

To examine the roles of the ERH-2/PICS-1 interface residues, we chose to mutate residues of PICS-1^{EBM} and examined their ERH-2 binding affinities by ITC. ITC binding data indicate that neither of PICS-1^{EBM} double mutants, I182D/V186D and V189D/L190D, displayed ERH-2 binding affinity, which confirms the roles of PICS-1 residues in binding to ERH-2 (**Fig. 3d-3e, Supplementary Table 1**).

Structure of TOST-1-bound ERH-2

ERH-2 also binds to the fragments of TOST-1 and PID-1 in a mutually exclusive manner (**Fig. 4a, Supplementary Table 1**), and either of them effectively interacts with ERH-2 in the presence of PICS-1^{EBM} (**Supplementary Table 1**). To understand the molecular mechanism how TOST-1 binds to ERH-2, we made a similar fusion protein by linking ERH-2(1-103) with a fragment of TOST-1(34-54) via a $(GSS)_6$ linker, crystallized the fusion protein and determined its structure at a 2.20 Å resolution (**Supplementary Table 2**). In the TOST-1-bound structure, the ERH-2 homodimer is similar to that in the PICS-1-bound one. However, only one TOST-1 molecule (aa 35-54) is visible in the structure and the crystal packing prevents the access of the second TOST-1 to the symmetrical site (**Supplementary Fig. 5**).

The TOST-1 fragment (TOST-1$^{34-54}$) adopts a helix structure with two extended ends, and the helix is accommodated into the oval-shape pocket of the ERH-2 dimer (**Fig. 4b-c**). The helix of TOST-1 (aa 39-48) interacts with both ERH-2 protomers, ERH-2^{A} and ERH-2^{B}, via hydrophobic and electrostatic interactions (**Fig. 4d**). Leu39, Phe43, and Leu46 of TOST-1 make extensive hydrophobic interactions with Val8^{A}, Trp22^{A}, Phe73^{A}, Tyr80^{A}, Leu10^{B}, and Met71^{B}. The main chain amides of Leu39 and Asn40 form are hydrogen bonded to the carboxyl groups of Asp67^{B}; The side chain carboxyl group of TOST-1 Asn40 is hydrogen bonded to the main chain amide group of Arg85^{B}; The guanidino group of Arg42 forms cation-π and salt bridge with the side chains of His6^{A} and Glu26^{A}, respectively (**Fig. 4d**). In addition to the helix-mediated interactions, the Arg36 of TOST-1 forms salt bridge with Asp24^{A}, and the Thr51 of TOST-1 also makes additional hydrophobic contacts with Phe73^{A} (**Fig. 4d**).

Then we superimposed the two ERH-2 complexes together after modeling the

other TOST-1 molecule based on symmetry. In the overlaid structures, two PICS-1^{EBM} and two TOST-1 occupy different surfaces of ERH-2 dimer (**Supplementary Fig. 6**), which is consistent with our structural analysis that ERH-2 interact with PICS-1^{EBM} and TOST-1 via different residues (**Supplementary Fig. 4a**). Collectively, the two solved ERH-2 complexes imply that ERH-2 homodimer acts as a scaffold to bridge two PICS subunits *in vitro*.

Next we mutated the residues at the ERH-2/TOST-1 interface to evaluate their roles in complex formation. By using ITC binding assay, we found that D67A of ERH-2, R42C and L39A/F43A of TOST-1, abolished the interaction between TOST-1 and ERH-2 (**Fig. 4e-4g**), whereas the ERH-2 D67A binds to PICS-1^{EBM} in a comparable affinity with the wild type (K_ds: 4.3 μM vs. 8.5 μM) (**Supplementary Table 1**). Taken together, the binding data and mutagenesis experiments suggest that the PICS-1, and TOST-1 or PID-1, are capable of binding to different surfaces of dimerized ERH-2 simultaneously.

Furthermore, we purified the complex consisting of ERH-2-$(GSS)_6$-TOST-1, PICS-1$^{EBM\text{-}RRM}$, and TOFU-6^{RRM} via the gel filtration assay, and the peak corresponding to the complex indicated the molecular weight (MW) of ~80 kD, consistent with a 2:2:2 complex (**Supplementary Fig. 7**). Therefore, we confirmed that the core PICS complex exists as an octamer containing two copies of each subunits.

Impact of interaction network on subcellular localizations

We further examined how the *in vivo* localizations of PICS subunits are affected by the interaction network that has been uncovered by *in vitro* experiments. Consistent with our previous work, TOFU-6 localizes at the perinuclear granule in germline cells, depending on PICS-1 (**Fig. 5a**)[39]. TOFU-6 D26A/W27A, which severely impairs the TOFU-6/PICS-1 interaction, is still in cytoplasm, but does not associate with perinuclear granules in germline cells (**Fig. 5a**). In contrast, TOFU-6 wild type and D26A/W27A mutant localize in the cytosol without association with granule in oocyte and embryos (**Supplementary Fig. 8**). PICS-1 is localized in cytosol in oocyte and

embryos (**supplementary Fig. 9a**), and associates with the perinuclear granules in germline cells (**Fig. 5b**). The PICS-1 F217E mutant, which disrupts the homodimerization, failed to associate with perinuclear granules (**Fig. 5c**). K246A/F247A and Y250A/Q251A of PICS-1 that remarkably weakened the PICS-1/TOFU-6 interaction, failed to associate with perinuclear granules but localized inside the nuclear envelope in germline cells (**Fig. 5c**), as evidenced by using lamin protein LMN-1::mCherry as the nuclear envelope marker (**Supplementary Fig. 9b**). In contrast, the three PICS-1 mutants exhibited the same localization as the wild type protein in oocyte and embryos (**Supplementary Fig. 9c**). For cells with *tofu-6* mutants, PICS-1 failed to accumulate at the perinuclear granules in the germline, but changed the localization from the cytoplasm to nucleus in embryos (**Fig. 5b and supplementary Fig. 10a**). Taken together, the localization of PICS-1 in the cytosol depends on TOFU-6, and the TOFU-6/PICS-1 interaction is critical for both proteins to associate with perinuclear granules.

Then we sought to examine how the PICS-1/ERH-2 interaction affects the localizations of both proteins. In germline cells, the two PICS-1 mutants eliminating the PICS-1/ERH-2 interaction, I182D/V186D, and V189D/L190D, form more and bigger perinuclear granules in cytoplasm in *pics-1* mutant background, similar to that of wild-type PICS-1 in *erh-2* mutant background (**Fig. 5b-5c**), indicating that the interaction between PICS-1 and ERH-2 plays an important role in controlling the level of PICS-1 in granules. ERH-2 associates with perinuclear granule in germline cells and is localized in cytoplasm in oocyte and embryos (**Fig. 5d and supplementary Fig. 10b**). *tofu-6* mutations that impair the TOFU-6/PICS-1 interaction, also resulted in a nuclear accumulation of ERH-2 in embryos (**supplementary Fig. 10b**), suggesting the key role of TOFU-6 in directing PICS-1/ERH-2 into perinuclear granules.

Next we studied the impact of ERH-2/TOST-1 interaction on their subcellular localizations. In germline cells, ERH-2 forms more and bigger granules in *tost-1* mutants than in wild type animals (**Fig. 5d**). TOST-1 localized at the cytoplasm of germline cells, oocytes, and embryos in wild type animals. In *erh-2* mutant, TOST-1 is

not expressed in the germline cells and embryos, but accumulated in the nucleus in oocytes (**Fig. 5d**). D67A of ERH-2 that disrupts the binding of ERH-2 to TOST-1 and PID-1, forms more granules in cytoplasm (**Fig. 5e**), suggesting that the binding of ERH-2 to TOST-1 or PID-1 mediates the assembly of ERH-2 associated perinuclear granules. L39A/F43A, and R42C of TOST-1, which abolish the ERH-2/TOST-1 interaction, are not expressed in germline cells and embryos, but accumulated in the nucleus in oocytes (**Fig. 5f**). Overall, the localizations of ERH-2 and TOST-1 are dependent on each other.

The mis-localizations of PICS subunits prompt us to investigate whether the mutants associated with aberrant perinuclear granule localization also have impact on piRNA biogenesis *in vivo*. We examined the levels of typical piRNAs by quantitative real-time PCR and found that those missense mutants, as well as the null mutants, all lead to impaired piRNA production *in vivo* (**Fig. 5g**). Collectively, intact interaction network within PICS is essential not only for the association with perinuclear granules, but also for piRNA biogenesis *in vivo*.

Intact PICS complex is required for chromosome segregation and cell division.

Consistent with our previous work that the TOST-1-containing PICS complex regulates embryonic chromosome segregation and cell division[39], null mutants of PICS subunits, such as *tofu-6(ust94), erh-2(ust101), pics-1(tm2417),* and *tost-1(ust103)*, all lead to delay and nondisjunction in chromosome segregation during cell division (**Fig. 6a-d**). In contrast with the null mutants of PICS subunits, the TOFU-6 mutant *ust173* (**Fig. 6a**), and three PICS-1 mutants (K245A/K246A, Y250A/Q251A, and F217E) do not have impact on chromosome segregation and cell division (**Fig. 6b**), suggesting that although TOFU-6 is essential, its interaction with PICS-1 is not required for chromosome segregation and cell division. It is likely that other TOFU-6 domains, such as the Tudor domain or the C-terminal region, mediate chromosome segregation and cell division.

Next we examined whether interactions between PICS-1, ERH-2 and TOST-1

are required for the maintenance of normal chromosome segregation during cell cycle. We found that two PICS-1mutants that disrupt PICS-1/ERH-2 interactions, I182D/V186D and V189D/L190D, display abnormal chromosome segregation and cell division (**Fig. 6b**). In addition, the mutants that abolish the ERH-2/TOST-1 interaction, including D67A of ERH-2 (**Fig. 6c**), L39A/F43Aand R42C of TOST-1 (**Fig. 6d**), all caused delay and nondisjunction in chromosome segregation and cell division. Consistently, the mutants associated with impaired chromosome segregation and cell division, also resulted in sterility of the animals (**Supplementary Fig. 11**). Therefore, our data indicate that the PICS-1-ERH-2-TOST-1 axis is critical for chromosome segregation, cell division, and fertility.

Discussion

piRNAs, named for being associated with PIWI proteins, play an important role in defending against non-self nucleic acids. In *C. elegans*, piRNAs are abundant in germline and necessary for fertility. Recently, a variety of protein complexes have been identified to be involved in piRNA biogenesis, including transcription, export, to maturation. PICS complex consists of four core subunits and was found to be involved into the medication of piRNA biogenesis and cell division via two mutually exclusive factors, PID-1 and TOST-1, respectively.

Here we present three structures for PICS subunits, including those of TOFU-6^{RRM}/PICS-1^{RRM}, ERH-2/PICS-1^{EBM}, and ERH-2/TOST-1, to uncover the mechanism underlying the PICS formation. *In vitro* biochemistry experiments support that PICS is an octamer composed of two copies of each four subunits. Combined with biochemical and mutagenesis experiments, our structural biology data unveil the assembly interface within PICS complex. The interactions between PICS subunits are critical for the proper localization of PICS *in vivo*, suggesting the localization of PICS units are dependent on each other. Unexpectedly, PICS-1 and TOFU-6 interact with each other via RRM domains, which were previously identified as the RNA binding modules. ERH-2 and PICS-1 are both homodimers within the PICS complex and the two homodimers interact with each other in a 2:2 ratio to form a homogenous tetramer rather than high-order polymers or aggregates, which constitutes the basis of PICS

octamer.

PICS complex has dual roles in piRNA biogenesis and chromosome segregation. The correct localizations of PICS subunit are interdependent. Specifically, the cytoplasmic localizations of the other PICS subunits are dependent on the interaction between TOFU-6 and PICS-1, suggesting the role of TOFU-6 in balancing the levels of PICS subunits between cytoplasm and nucleus. Intriguingly, the TOFU-6/PICS-1 interaction is important for piRNA biogenesis, but not required for chromosome segregation, although TOFU-6 is essential for chromosome segregation, one explanation could be that TOFU-6 might mediate chromosome segregation via its N-terminal MID domain or C-terminal IFE-3 binding motif. In contrast, the interactions between PICS-1, ERH-2 and TOST-1 are essential in chromosome segregation during cell division. Therefore, PICS mediates cell division via the PICS-1/ERH-2/TOST-1 axis, in which ERH-2 dimer acts as the scaffold to tether PICS-1 and TOST-1. Combining structural biology with biochemistry and mutagenesis experiments, we confirmed that a shared surface of ERH-2 dimer mediates the binding of TOST-1 or PID-1, allowing PICS complex to make a choice in being involved into piRNA biogenesis or cell division.

The ligand binding modes of ERH-2 in different eukaryotic species

ERH-2 is the only conserved subunit in PICS complex among eukaryotic species. The overall structure of ERH-2, as well as the dimer interface, are conserved from yeast to human (**Supplementary Fig. 4a**). Recently, two eukaryotic ERH-2 complexes were solved, including the structures of human ERH bound with a fragment of DGCR8, and of *Schizosaccharomyces pombe* Erh1 with Mmi1, which prompts us to compare the structures of *C. elegans* ERH-2 with its orthologs. In all structures, ERH form homodimer and bind to ligands in a 2:2 ratio. In the overlaid structures, we found that although ERH orthologs utilize similar surface to bind their ligands, the ligands exhibit different conformations upon binding to different ERH orthologs (**Supplementary Fig. 4b**). Despite that the DGCR8 fragment overlaps with PICS-1^{EBM}, it exhibits extended conformation whereas the PICS-1^{EBM} adopts a helix.

It is possible that some unknown protein might interact with human ERH via the TOST-1 binding site (**Supplementary Fig. 4b**). The N-terminal and C-terminal fragments of *Schizosaccharomyces pombe* Mmi1 overlaps with TOST-1 and PICS-1^{EBM}, respectively. While the N-terminal fragment of Mmi1 adopts a distorted helix, TOST-1 demonstrates a regular helix structure with two extended fragments at both ends. The C-terminal of Mmi1 exhibits an extended conformation, different from that of PICS-1^{EBM} (**Supplementary Fig. 6**). It is noteworthy that neither of the *C. elegans* ERH-2 binding ligands are conserved in *homo sapiens* or *Schizosaccharomyces pombe*, and *vice versa*. Despite the versatile ligand binding modes for ERH proteins from different species, ERH dimer likely maintains the conserved role as the scaffold through keeping the surfaces for dimerization and for ligand binding during evolution.

Overall our structural biology work, combined with biochemistry, cell biology and imaging experiments, not only unveils the mechanism underlying the roles of PICS-1 and ERH-2 as scaffolds within the PICS complex, but also provides insights into understanding the dual functions of PICS through targeting one of the two mutually exclusive factors, PID-1 or PICS-1, with ERH-2 dimer. Therefore, the existence of PICS-like complex might reflect the requirement of higher eukaryotes for accurately mediating the balance between key cellular events, such as piRNA biogenesis and cell division.

Methods

Cloning, mutations, protein expression and purification.

Gene encoding full-length *C. elegans* TOFU-6, PICS-1, TOST-1 and PID-1 were codon-optimized for expression in *Escherichia coli* and synthesized by Sangon Biotech. ERH-2 was amplified by PCR from the *C. elegans* cDNA library. TOFU-6^{RRM}(residues 2-92) and PICS-1^{RRM} (residues 201-282) were cloned into upstream and downstream multiple cloning sites of a modified pETDuet-1 (Novagen). ERH-2$^{2-103}$-(Gly-Ser-Ser)$_7$-PICS-1$^{180-200}$ and ERH-2$^{2-103}$-(Gly-Ser-Ser)$_6$-TOST-1$^{34-54}$ fusion clone were constructed by overlap extension PCR. PICS-1^{EBM} (residues

180-200) and a TOST-1 fragment (residues 34-54) were cloned into pET28-SUMO vector (Invitrogen™).

Recombinant proteins were over-expressed in *Escherichia coli* BL21(DE3). Cells were grown in LB medium at 37 °C until the optical density (OD_{600}) reached ~0.8. Protein expression was induced with 0.2 mM β-d-1-thiogalactopyranoside for 20 h at 16 °C. Cells were gathered by centrifuge at 3,600 g for 10 min at 4 °C, and pellets were resuspended in lysis buffer containing 20 mM Tris-HCl, pH 7.5, 400 mM NaCl.

All recombinant proteins were purified firstly by Ni-NTA (GE healthcare). TOFU-6/PICS-1 was further purified by HiLoad 16/600 Superdex 75 column (GE healthcare) in a buffer containing 20 mM Tris-HCl, pH8.5, 200 mM NaCl. Seleno-methionine (SeMet) labeled TOFU-6/PICS-1 was purified in the same way as native proteins, except that cells were cultured in M9 medium supplied with 50 mg/L of SeMet. ERH-$2^{2\text{-}103}$-$(\text{Gly-Ser-Ser})_7$-PICS-$1^{180\text{-}200}$ and ERH-$2^{2\text{-}103}$-$(\text{Gly-Ser-Ser})^6$-TOST-$1^{34\text{-}54}$ were further purified by HiLoad 16/600 Superdex 75 column (GE healthcare) in a buffer containing 20 mM MES, pH6.5, 200 mM NaCl.

Site-specific mutations were performed using two reverse and complement primers containing the mutation codon. Primer sets used for mutations are listed in Supplementary Table 5. The mutants of TOFU-6^{RRM}, PICS-1^{RRM}, and ERH-2 were cloned into the pET28-MHL vector , while the mutants of PICS-1^{EBM} and TOST-1 were cloned into the pET28-SUMO vector. All mutants were purified in the same way as wild-type proteins.

Crystallization data collection and structure determination.

Protein crystals were grown at 18 °C by sitting drop vapor diffusion method. For crystallization, 1 μl of protein solution was mixed with 1 μl of crystallization buffer. TOFU-6/PICS-1 complex were concentrated to 10–15 mg ml^{-1} in a buffer containing 20 mM Tris-HCl, pH 8.5, 200 mM NaCl; ERH-$2^{2\text{-}103}$-$(\text{Gly-Ser-Ser})_7$-PICS-$1^{180\text{-}200}$ and ERH-$2^{2\text{-}103}$-$(\text{Gly-Ser-Ser})_6$-TOST-$1^{34\text{-}54}$ were concentrated to 10–15 mg ml^{-1} in a

buffer containing 20 mM MES, pH 6.5, 200 mM NaCl. Crystals were obtained as follows:

(1) Native TOFU-6^{RRM}/PICS-1^{RRM} complex was crystallized in a buffer containing 0.1M Tris hydrochloride, pH 8.5, 2 M Ammonium sulfate.

(2) SeMet TOFU-6^{RRM}/PICS-1^{RRM} complex was crystallized in a buffer containing 2% (v/v) 1,4-Dioxane, 0.1 M Tris hydrochloride, pH 8.0 , 15 % PEG 3350 and 0.01 M Nickel (ll) chloride hexahydrate.

(3) ERH-2$^{2-103}$-(Gly-Ser-Ser)$_7$-PICS-1$^{180-200}$ was crystallized in a buffer containing 15% (v/v) 2-propanol , 0.1 M sodium citrate tribasic dehydrate, pH 5.0 and 10% PEG 10000.

(4) ERH-2$^{2-103}$-(Gly-Ser-Ser)$_6$-TOST-1$^{34-54}$ was crystallized in a buffer containing 0.1 M Bis-tris, pH 6.2, 20% tascimate (pH6.0).

Before flash-freezing crystals in liquid nitrogen, all crystals were soaked in a cryo-protectant consisting of 85 % reservoir solution plus 15 % glycerol. The diffraction data were collected on beamline BL18U1 and BL19U1 [43] at Shanghai Synchrotron Facility. The statistic details about data collection are summarized in Supplementary Table 1. Data sets were processed using HKL2000/3000 [44, 45] or XDS[46]. The initial model of SetMet TOFU-6/PICS-1 complex was solved by CRANK2 [47], built manually by COOT[48], and refined by Phenix[49]. Structure of native TOFU-6/PICS-1 was solved by Phenix[49] with the SeMet structure as the search model for molecular replacement. ERH-2$^{2-103}$-(Gly-Ser-Ser)$_7$-PICS-1$^{180-200}$ and ERH-2$^{2-103}$-(Gly-Ser-Ser)$_6$-Tost-1$^{34-54}$ structures were solved by molecular replacement with human ERH protein (PDB ID: 1WZ7) as the search model and were further refined by Phenix[49].

Isothermal titration calorimetry (ITC)

ITC binding assays were carried out on a MicroCal ITC200 calorimeter (GE Healthcare) at 25 °C in a buffer containing 20 mM Tris, pH 7.5, 200 mM NaCl. Before ITC experiments, all purified proteins were dialyzed against ITC buffer. ITC experiments were performed by titrating 2 μl of proteins or peptides in the syringe

(1–2 mM) into the cell containing 30–50 μM proteins, with a spacing time of 120 s and a reference power of 5 μCal s^{-1}. Control experiments were performed by titrating proteins or peptides (1–2 mM) into the ITC buffer, and were subtracted during analysis, respectively. Binding isotherms were plotted, analyzed and fitted based on one-site binding model by MicroCal PEAQ-ITC Analysis software (Malvern Panalytical). The dissociation constants (Kd) and peptide sequences used for ITC experiments are summarized in Supplementary Table 2, and representative ITC binding curves are shown in Supplementary Fig. 12.

Gel filtration assay

For gel filtration experiment, the wide type and mutant (F217E) of PICS-1^{RRM} were purified in by HiLoad 16/600 Superdex 75 column in a buffer containing 20 mM Tris hydrochloride, pH 7.5, and 200 mM NaCl, respectively. A complex consisting of ERH-$2^{2\text{-}103}$-$(GSS)_6$- TOST-$1^{34\text{-}54}$, PICS-$1^{EBM\text{-}RRM}$, and TOFU-6^{RRM} was purified by HiLoad 16/600 Superdex 200 column (GE healthcare) in a buffer containing 20 mM Tris hydrochloride, pH 7.5, 200 mM NaCl.

Construction of transgenic mutant strains.

For wild-type and amino acids substituted GFP tagged transgenes, endogenous promoter sequences, ORFs or amino acids substituted ORFs, coding sequence for gfp::3xflag, 3' UTR, and a linker sequence (GGAGGTGGAGGTGGAGCT) (inserted between the ORFs and gfp::3xflag) were fused and cloned into PCFJ151 vectors using a ClonExpress MultiS One Step Cloning Kit (Vazyme C113-02, Nanjing). These transgenes were integrated into the *C. elegans'* chromosome II or V by MosSCI technology.

For *tofu-6(ust173)* mutant, sgRNAs closed to the substituted bases and the repair template were co-injected into N2 animals with PDD162 (50 ng/μL), pcfj90 (20 ng/μL), 10xTE buffer, and DNA ladder (500 ng/μL). The repair template that contains homologous arms of 1000 bp to 1500 bp and substituted base pairings were cloned into a vector using the ClonExpress MultiS One Step Cloning Kit. Two or three days later, F1 worms expressing the pcfj90 marker were isolated. After growing at 20°C for another three days, the animals were screened for base pairing substitution by

PCR and restriction enzyme reaction.

Microscope and images.

Images were collected on Leica DM4B microscope.

RNA isolation.

Synchronized young adult worms were collected and sonicated in the sonication buffer containing 20 mM Tris hydrochloride, pH 7.5, 200 mM NaCl, 2.5 mM $MgCl_2$, and 0.5% NP40). The eluates were incubated with TRIzol reagent and then precipitated with isopropanol. The precipitated nucleic acids were treated with DNase I, re-extracted with TRIzol and then precipitated with isopropanol again. The concentrations of RNA were measured using Nano Drop.

RT-qPCR.

RNA was isolated from the indicated animals and subjected to DNase I digestion (Thermo Fisher). cDNA was generated from the RNA using a *GoScript™ Reverse Transcription System* (Promega) according to the vendor's protocol. qPCR was performed using a MyIQ2 real-time PCR system (Bio-Rad) with AceQ SYBR Green Master mix (Vazyme). Total reverse transcribed RNA levels were used as an internal control for sample normalization.

Brood size.

L3 worms were placed individually into fresh NGM plates, and the progeny numbers were scored.

Statistics.

Bar graphs with error bars represented the mean and SD. All of the experiments were conducted with independent *C. elegans* animals for the indicated N replicates. Statistical analysis was performed with two-tailed Student's t-tests or unpaired Wilcoxon tests. Student's t-test p value threshold was set to 0.05.

Acknowledgements

We thank the staffs from BL17B/BL18U1/BL19U1/BL19U2/BL01B beamline of National Facility for Protein Science in Shanghai (NFPS) at Shanghai Synchrotron Radiation Facility, for assistance during data collection. This work was supported by

the "Strategic Priority Research Program" of the Chinese Academy of Sciences (Grant No. XDB19000000), the National Key R&D Program of China (2019YFA0802600, 2018YFC1004500, and 2017YFA0102900), and National Natural Science Foundation of China Grants (31770806, 92053107). C. X. is also supported by supported by "the Fundamental Research Funds for the Central Universities" and "the Thousand Young Talent program".

Author contributions

C.X. and S.G. conceived the project. X.W. and S.L. performed structural biology and biochemical experiments with assistance from Z.Z., X.T., and J.Z.. C.Z. and X.F. performed *in vivo* experiments. C.X. and S.G. wrote the manuscript. All authors contributed to editing the manuscript. C.X. and S.G. supervised the project.

Data availability

Atomic coordinates and structure factors for structures of SeMet TOFU-6^{RRM}(L73M)/PICS-1^{RRM}(I233M), native TOFU-6^{RRM}/PICS-1^{RRM}, ERH-2/PICS-1^{EBM}, and ERH-2/TOST-1 were deposited into Protein Data Bank under accession codes 7D1L, 7D2Y, 7EJS, and 7EJO, respectively.

Competing interests

The authors declare no competing interests.

Additional information

Extended data is available for this paper at xxxxx.

Supplementary information is available for this paper at xxxxx.

References

1. Aravin AA, Naumova NM, Tulin AV, Vagin VV, Rozovsky YM, Gvozdev VA. Double-stranded RNA-mediated silencing of genomic tandem repeats and transposable elements in the D. melanogaster germline. *Curr Biol* **11**, 1017-1027 (2001).

2. Ozata DM, Gainetdinov I, Zoch A, O'Carroll D, Zamore PD. PIWI-interacting RNAs: small RNAs with big functions. *Nat Rev Genet* **20**, 89-108 (2019).

3. Weick EM, Miska EA. piRNAs: from biogenesis to function. *Development* **141**, 3458-3471

(2014).

4. Almeida MV, Andrade-Navarro MA, Ketting RF. Function and Evolution of Nematode RNAi Pathways. *Non-coding RNA* **5**, (2019).

5. Sato K, Siomi MC. The piRNA pathway in Drosophila ovarian germ and somatic cells. *Proceedings of the Japan Academy Series B, Physical and biological sciences* **96**, 32-42 (2020).

6. Cox DN, Chao A, Baker J, Chang L, Qiao D, Lin H. A novel class of evolutionarily conserved genes defined by piwi are essential for stem cell self-renewal. *Genes & development* **12**, 3715-3727 (1998).

7. Deng W, Lin H. miwi, a murine homolog of piwi, encodes a cytoplasmic protein essential for spermatogenesis. *Developmental cell* **2**, 819-830 (2002).

8. Gou LT*, et al.* Ubiquitination-Deficient Mutations in Human Piwi Cause Male Infertility by Impairing Histone-to-Protamine Exchange during Spermiogenesis. *Cell* **169**, 1090-1104.e1013 (2017).

9. Kuramochi-Miyagawa S*, et al.* Mili, a mammalian member of piwi family gene, is essential for spermatogenesis. *Development (Cambridge, England)* **131**, 839-849 (2004).

10. Carmell MA*, et al.* MIWI2 is essential for spermatogenesis and repression of transposons in the mouse male germline. *Developmental cell* **12**, 503-514 (2007).

11. Shen EZ*, et al.* Identification of piRNA Binding Sites Reveals the Argonaute Regulatory Landscape of the C. elegans Germline. *Cell* **172**, 937-951.e918 (2018).

12. Zhang D*, et al.* The piRNA targeting rules and the resistance to piRNA silencing in endogenous genes. *Science (New York, NY)* **359**, 587-592 (2018).

13. Malone CD*, et al.* Specialized piRNA pathways act in germline and somatic tissues of the Drosophila ovary. *Cell* **137**, 522-535 (2009).

14. Ashe A*, et al.* piRNAs can trigger a multigenerational epigenetic memory in the germline of C. elegans. *Cell* **150**, 88-99 (2012).

15. Shirayama M*, et al.* piRNAs initiate an epigenetic memory of nonself RNA in the C. elegans germline. *Cell* **150**, 65-77 (2012).

16. Bagijn MP*, et al.* Function, targets, and evolution of Caenorhabditis elegans piRNAs. *Science (New York, NY)* **337**, 574-578 (2012).

17. Lee HC, Gu W, Shirayama M, Youngman E, Conte D, Jr., Mello CC. C. elegans piRNAs mediate

the genome-wide surveillance of germline transcripts. *Cell* **150**, 78-87 (2012).

18. Luteijn MJ, Ketting RF. PIWI-interacting RNAs: from generation to transgenerational epigenetics. *Nature reviews Genetics* **14**, 523-534 (2013).

19. Das PP*, et al.* Piwi and piRNAs act upstream of an endogenous siRNA pathway to suppress Tc3 transposon mobility in the Caenorhabditis elegans germline. *Molecular cell* **31**, 79-90 (2008).

20. Batista PJ*, et al.* PRG-1 and 21U-RNAs interact to form the piRNA complex required for fertility in C. elegans. *Mol Cell* **31**, 67-78 (2008).

21. Wang G, Reinke V. A C. elegans Piwi, PRG-1, regulates 21U-RNAs during spermatogenesis. *Current biology : CB* **18**, 861-867 (2008).

22. Gu SG, Pak J, Guang S, Maniar JM, Kennedy S, Fire A. Amplification of siRNA in Caenorhabditis elegans generates a transgenerational sequence-targeted histone H3 lysine 9 methylation footprint. *Nature genetics* **44**, 157-164 (2012).

23. Mao H*, et al.* The Nrde Pathway Mediates Small-RNA-Directed Histone H3 Lysine 27 Trimethylation in Caenorhabditis elegans. *Current biology : CB* **25**, 2398-2403 (2015).

24. Suen KM*, et al.* DEPS-1 is required for piRNA-dependent silencing and PIWI condensate organisation in Caenorhabditis elegans. *Nature communications* **11**, 4242 (2020).

25. Ruby JG*, et al.* Large-scale sequencing reveals 21U-RNAs and additional microRNAs and endogenous siRNAs in C. elegans. *Cell* **127**, 1193-1207 (2006).

26. Gu W*, et al.* CapSeq and CIP-TAP identify Pol II start sites and reveal capped small RNAs as C. elegans piRNA precursors. *Cell* **151**, 1488-1500 (2012).

27. Weick EM*, et al.* PRDE-1 is a nuclear factor essential for the biogenesis of Ruby motif-dependent piRNAs in C. elegans. *Genes & development* **28**, 783-796 (2014).

28. Kasper DM, Wang G, Gardner KE, Johnstone TG, Reinke V. The C. elegans SNAPc component SNPC-4 coats piRNA domains and is globally required for piRNA abundance. *Developmental cell* **31**, 145-158 (2014).

29. Goh WS, Seah JW, Harrison EJ, Chen C, Hammell CM, Hannon GJ. A genome-wide RNAi screen identifies factors required for distinct stages of C. elegans piRNA biogenesis. *Genes Dev* **28**, 797-807 (2014).

30. Weng C*, et al.* The USTC co-opts an ancient machinery to drive piRNA transcription in C. elegans. *Genes Dev* **33**, 90-102 (2019).

31. Beltran T, Pahita E, Ghosh S, Lenhard B, Sarkies P. Integrator is recruited to promoter-proximally paused RNA Pol II to generate Caenorhabditis elegans piRNA precursors. *EMBO J*, e105564 (2020).

32. Berkyurek AC*, et al.* The RNA polymerase II subunit RPB-9 recruits the integrator complex to terminate Caenorhabditis elegans piRNA transcription. *EMBO J*, e105565 (2021).

33. Choi CP*, et al.* SNPC-1.3 is a sex-specific transcription factor that drives male piRNA expression in C. elegans. *eLife* **10**, (2021).

34. Tang W, Tu S, Lee HC, Weng Z, Mello CC. The RNase PARN-1 Trims piRNA 3' Ends to Promote Transcriptome Surveillance in C. elegans. *Cell* **164**, 974-984 (2016).

35. Billi AC*, et al.* The Caenorhabditis elegans HEN1 ortholog, HENN-1, methylates and stabilizes select subclasses of germline small RNAs. *PLoS genetics* **8**, e1002617 (2012).

36. Kamminga LM*, et al.* Differential impact of the HEN1 homolog HENN-1 on 21U and 26G RNAs in the germline of Caenorhabditis elegans. *PLoS genetics* **8**, e1002702 (2012).

37. Montgomery TA*, et al.* PIWI associated siRNAs and piRNAs specifically require the Caenorhabditis elegans HEN1 ortholog henn-1. *PLoS genetics* **8**, e1002616 (2012).

38. Cordeiro Rodrigues RJ*, et al.* PETISCO is a novel protein complex required for 21U RNA biogenesis and embryonic viability. *Genes Dev* **33**, 857-870 (2019).

39. Zeng C*, et al.* Functional Proteomics Identifies a PICS Complex Required for piRNA Maturation and Chromosome Segregation. *Cell Rep* **27**, 3561-3572 e3563 (2019).

40. de Albuquerque BF*, et al.* PID-1 is a novel factor that operates during 21U-RNA biogenesis in Caenorhabditis elegans. *Genes Dev* **28**, 683-688 (2014).

41. Minasaki R, Streit A. MEL-47, a novel protein required for early cell divisions in the nematode Caenorhabditis elegans. *Molecular genetics and genomics : MGG* **277**, 315-328 (2007).

42. Maris C, Dominguez C, Allain FH. The RNA recognition motif, a plastic RNA-binding platform to regulate post-transcriptional gene expression. *FEBS J* **272**, 2118-2131 (2005).

43. Zhang WZ, Tang JC, Wang SS, Wang ZJ, Qin WM, He JH. The protein complex crystallography beamline (BL19U1) at the Shanghai Synchrotron Radiation Facility. *Nucl Sci Tech* **30**, (2019).

44. Otwinowski Z, Minor W. Processing of X-ray diffraction data collected in oscillation mode. *Methods Enzymol* **276**, 307-326 (1997).

45. Minor W, Cymborowski M, Otwinowski Z, Chruszcz M. HKL-3000: the integration of data

reduction and structure solution--from diffraction images to an initial model in minutes. *Acta Crystallogr D Biol Crystallogr* **62**, 859-866 (2006).

46. Kabsch W. Xds. *Acta Crystallogr D Biol Crystallogr* **66**, 125-132 (2010).

47. Pannu NS, Waterreus WJ, Skubak P, Sikharulidze I, Abrahams JP, de Graaff RA. Recent advances in the CRANK software suite for experimental phasing. *Acta Crystallogr D Biol Crystallogr* **67**, 331-337 (2011).

48. Emsley P, Cowtan K. Coot: model-building tools for molecular graphics. *Acta Crystallogr D Biol Crystallogr* **60**, 2126-2132 (2004).

49. Adams PD*, et al.* PHENIX: building new software for automated crystallographic structure determination. *Acta Crystallogr D Biol Crystallogr* **58**, 1948-1954 (2002).

Figure legends

Figure 1. Interaction network within PICS complex. a Domain architecture of PICS subunits, TOFU-6, PICS-1, ERH-2, and TOST-1 or PID-1. Interactions between PICS subunits are indicated by black dash arrows. Functions of TOST-1- and PID-1-containing complexes are different. **b** ITC binding curves for PICS-1^{RRM} binding to TOFU-6^{RRM}. **c** Overall structure of TOFU-6^{RRM}/ PICS-1^{RRM} heterotetramer. Two PICS-1^{RRM} molecules are shown in red and cyan cartoon, respectively, while the two TOFU-6^{RRM} molecules are shown in orange and green cartoon, respectively. **d** Interface of PICS-1 ^{RRM} homodimer. Two PICS-1^{RRM} molecules are shown in the same way as in Fig. 1c. **e** Detailed interactions between two PICS-1 ^{RRM} protomers in the dimer. Residues involved in intermolecular interactions are shown in sticks and hydrogen bonds are shown in black dashes.

Figure 2. The PICS-1^{RRM} dimer bind to Two TOFU-6^{RRM} molecules. a The electrostatic surface of the PICS-1^{RRM} dimer bound with TOFU-6^{RRM}. Due to symmetry, only one TOFU-6^{RRM} molecule, TOFU-6^{C} is shown in orange cartoon. **b-c,** Detailed interactions between TOFU-6^{C} and one PICS-1 protomer, PICS-1^{A}. **d** Detailed interactions between TOFU-6^{C} and the other PICS-1 protomer, PICS-1^{B}. In Fig. 2b-d, residues involved in TOFU-6/PICS-1 interaction are shown in sticks.

Hydrogen bonds are shown in black dashes. **e-f** ITC binding curves for mutants of PICS-1^{RRM} binding to TOFU-6^{RRM}. **g** ITC binding curves for PICS-1^{RRM} binding to TOFU-6^{RRM} mutant.

Figure 3. The structure of ERH-2 dimer bound with PICS-1^{EBM}. a ITC binding curves for PICS-1^{EBM} binding to ERH-2. **b** Overall structure of the ERH-2 dimer with two PICS-1^{EBM}. The two protomers in ERH-2 dimer, ERH-2^{A} and ERH-2^{B}, are shown in green and blue cartoon, respectively. Two PICS-1^{EBM} molecules, PICS-1^{C}, and PICS-1^{D}, that bind to the ERH-2 dimer symmetrically, are shown in brown cartoon. **c** Detailed interactions between PICS-1^{C} and ERH-2 dimer. Residues involved in ERH-2/PICS-1 interaction are shown in sticks. Hydrogen bonds are shown in black dashes. **d-e** ITC binding curves for PICS-1^{EBM} mutants binding to ERH-2.

Figure 4. The structure of ERH-2 dimer with TOST-1$^{34-54}$. ITC binding curves for TOST-1$^{34-54}$ binding to ERH-2. **b** Overall structure of the ERH-2 dimer with one TOST-1$^{34-54}$, with the other TOST-1$^{34-54}$ blocked by crystal packing. ERH-2 dimer are shown in the same way as in Fig. 3b, and invisible loop regions of ERH-2 dimer are indicated by dashes. **c** Electrostatic surface of ERH-2 dimer bound to TOST-1$^{34-54}$. **d** Detailed interactions between TOST-1$^{34-54}$ and ERH-2 dimer. Residues involved in ERH-2/TOST-1 interaction are shown in sticks. Hydrogen bonds are shown in black dashes. **e** ITC binding curves for TOST-1$^{34-54}$ binding to the ERH-2 D67A. **f-g** ITC binding curves for mutants of TOST-1$^{34-54}$ binding to ERH-2.

Figure 5. PICS promoting 21U RNAs biogenesis are dependent of the interactions of PICS subunits. **a** Images of adult germline cells expressing GFP tagged-TOFU-6 or TOFU-6 D26A/W27A in indicated mutant backgrounds. TOFU-6 D26A/W27A impairs the interaction between TOFU-6 and PICS-1. **b** Images of adult germline cells expressing GFP tagged- PICS-1 in indicated mutant backgrounds. **c** Images of adult germline cells expressing GFP tagged wild-type or amino acids-substituted PICS-1 in *pics-1 (tm2417)* background. K245A/F246A and Y250A/Q251A of PICS-1 weaken the interaction between TOFU-6 and PICS-1. F217E of PICS-1 disrupts the homodimerization of PICS-1. I182D/V186D and V189D/L190D of PICS-1disrupt the interaction between PICS-1 and ERH-2. **d**

Images of adult germline cells, oocytes and embryos expressing GFP tagged ERH-2 or TOST-1 in indicated mutant backgrounds. **e** Images of adult germline cells, oocytes and embryos expressing GFP tagged wild-type or amino acids- substituted ERH-2 in *erh-2* null mutant background. ERH-2 D67A disrupts the interaction between ERH-2 and TOST-1. **f** Images of adult germline cells, oocytes and embryos expressing GFP tagged wild-type or amino acids- substituted TOST-1 in *tost-1* null mutant background. L39A/F43A and R42C of TOST-1 disrupt the interaction between ERH-2 and TOST-1. **g** 21U-RNA levels are detected by quantitative RT-PCR. RNA levels are normalized to total reverse transcribed RNA. Mean ± SD; ***p<0.001, **p<0.01, *p<0.05; ns, not significant; n=4 replicates. Scale bars, 20 μm.

Figure 6. Disruption of the PICS-1/ERH-2 or ERH-2&TOST-1 interaction, but not the TOFU-6/PICS-1 interaction, leads to defects of chromosome segregation and cell division. a-d Images of GFP or mCherry tagged HIS-58 at the meta-anaphase in embryos in indicated backgrounds.

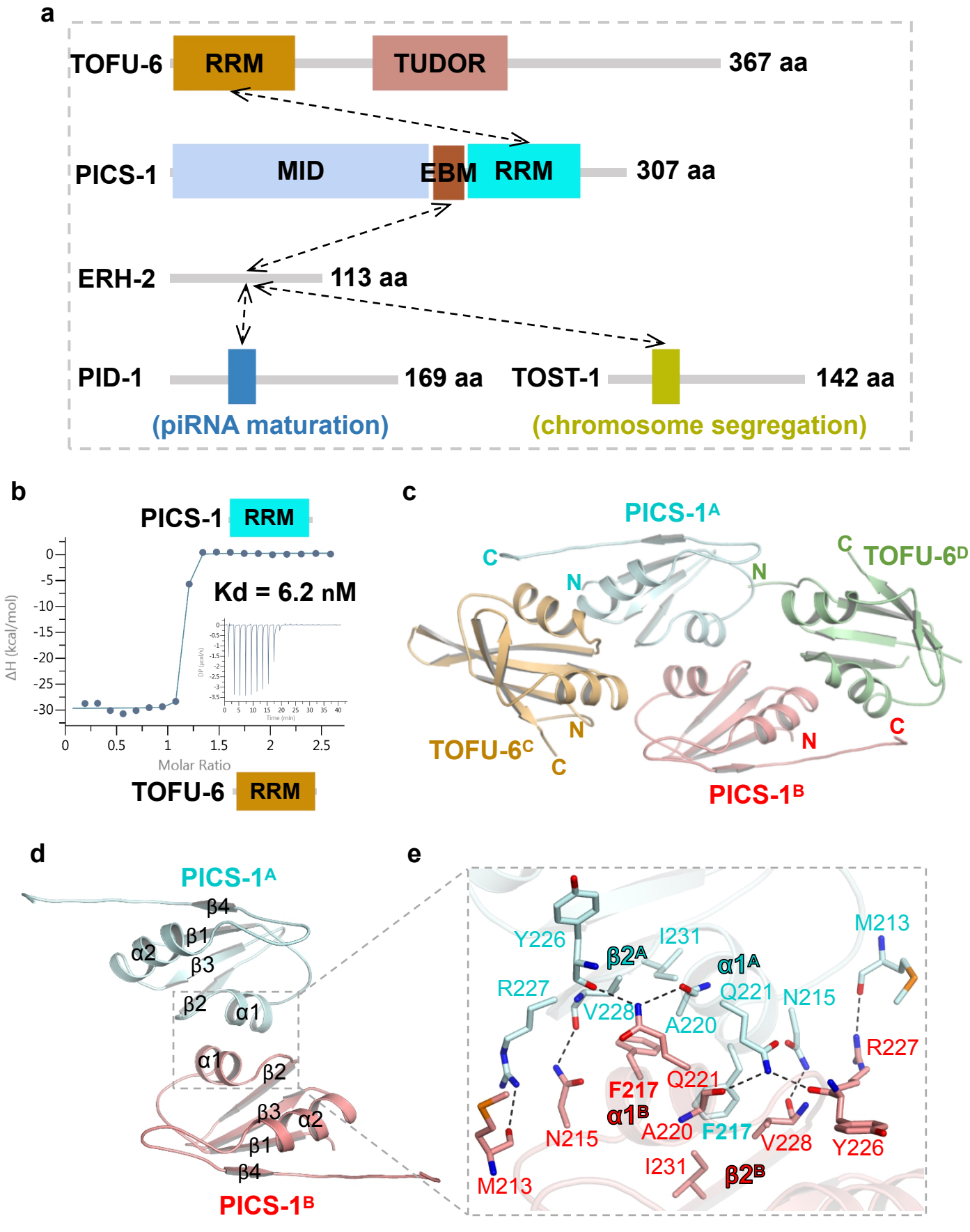
a
TOFU-6
RRM
TUDOR
367 aa
PICS-1
MID
EBM
RRM
307 aa
ERH-2
113 aa
PID-1
169 aa
TOST-1
142 aa
(piRNA maturation)
(chromosome segregation)
b
PICS-1
RRM
Kd = 6.2 nM
ΔH (kcal/mol)
Molar Ratio
TOFU-6
RRM
c
PICS-1A
TOFU-6D
TOFU-6C
PICS-1B
d
PICS-1A
β4
β1
α2
β3
β2
α1
α1
β2
β3
α2
β1
β4
PICS-1B
e
Y226
I231
β2A
α1A
M213
R227
Q221
N215
V228
A220
R227
F217
Q221
α1B
N215
A220
F217
V228
Y226
I231
β2B
M213

Figure 1

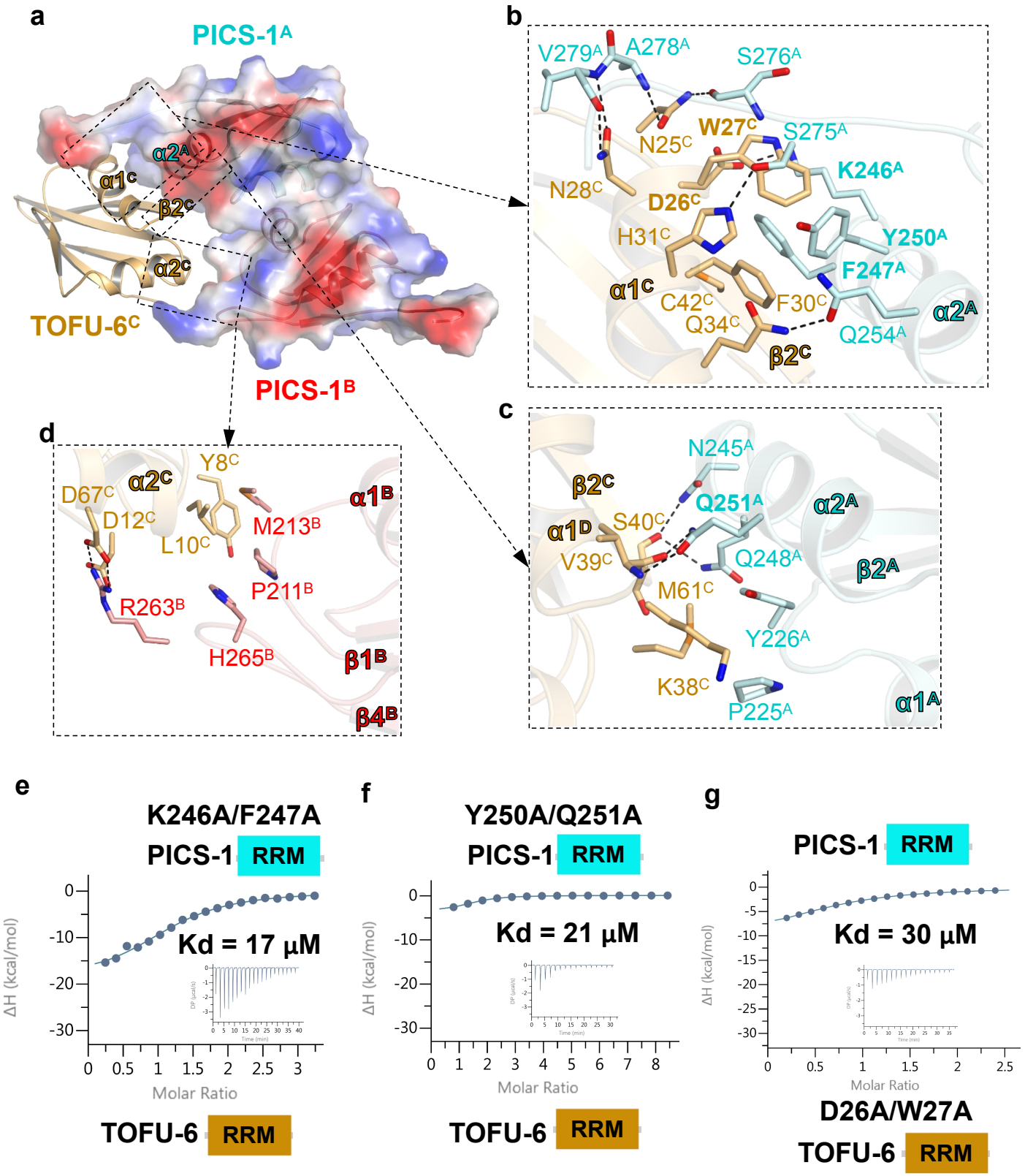
a
PICS-1A
α2A
α1C
β2C
α2C
TOFU-6C
PICS-1B
b
V279A
A278A
S276A
W27C
N25C
S275A
K246A
N28C
D26C
H31C
Y250A
F247A
α1C
C42C
F30C
α2A
Q34C
Q254A
β2C
c
N245A
β2C
Q251A
α2A
α1D
S40C
V39C
Q248A
β2A
M61C
Y226A
K38C
P225A
α1A
d
Y8C
D67C
α2C
α1B
D12C
M213B
L10C
P211B
R263B
H265B
β1B
β4B
e
K246A/F247A
PICS-1 RRM
Kd = 17 μM
ΔH (kcal/mol)
Molar Ratio
TOFU-6 RRM
f
Y250A/Q251A
PICS-1 RRM
Kd = 21 μM
ΔH (kcal/mol)
Molar Ratio
TOFU-6 RRM
g
PICS-1 RRM
Kd = 30 μM
ΔH (kcal/mol)
Molar Ratio
D26A/W27A
TOFU-6 RRM

Figure 2

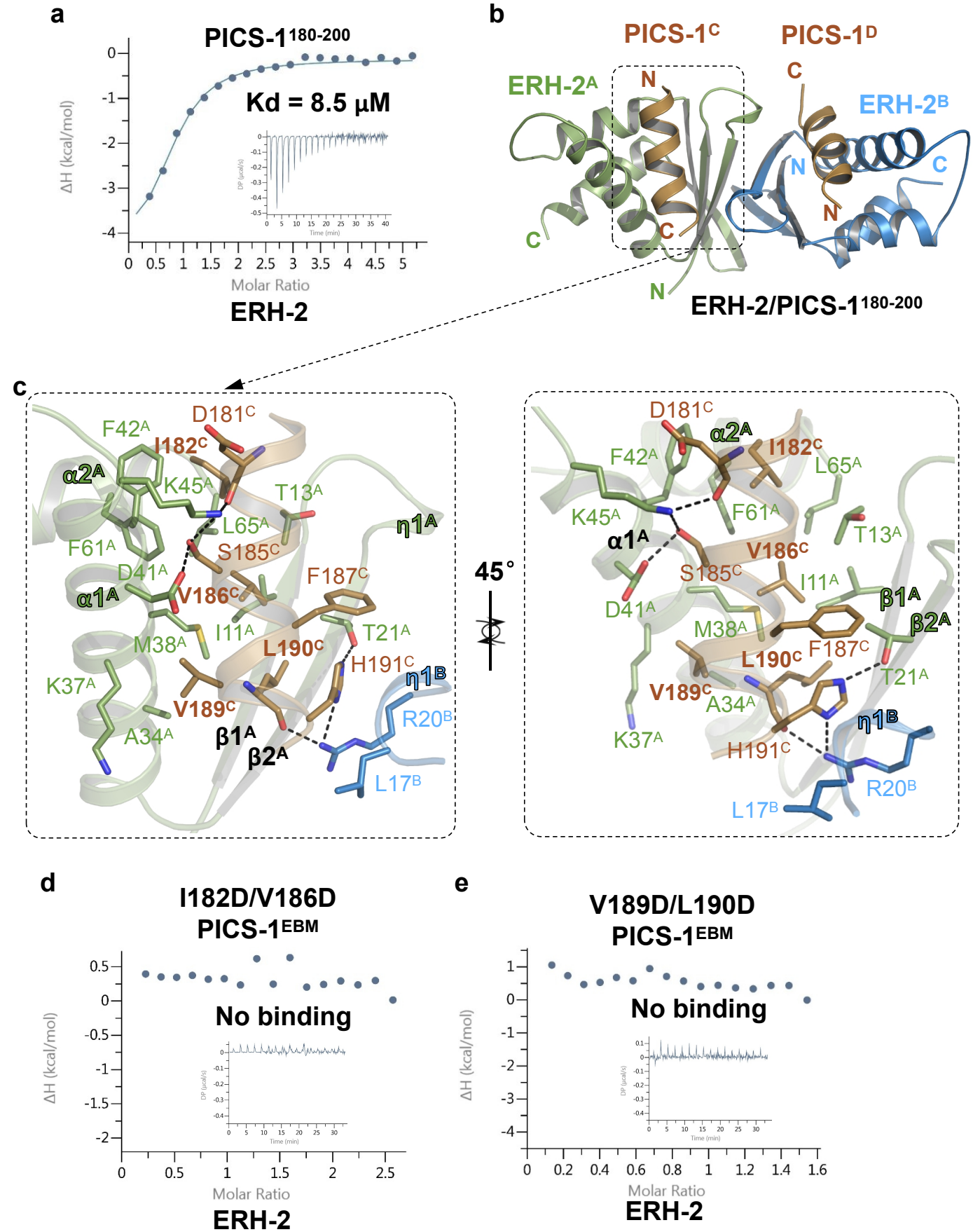
a
PICS-1180-200
Kd = 8.5 µM
ΔH (kcal/mol)
Molar Ratio
ERH-2
b
PICS-1C
PICS-1D
ERH-2A
ERH-2B
N
C
ERH-2/PICS-1180-200
c
D181C
F42A
I182C
α2A
K45A
T13A
L65A
η1A
F61A
S185C
D41A
α1A
V186C
F187C
I11A
T21A
M38A
L190C
H191C
η1B
K37A
V189C
R20B
A34A
β1A
β2A
L17B
45°
d
I182D/V186D
PICS-1EBM
No binding
ERH-2
e
V189D/L190D
PICS-1EBM
No binding
ERH-2

Figure 3

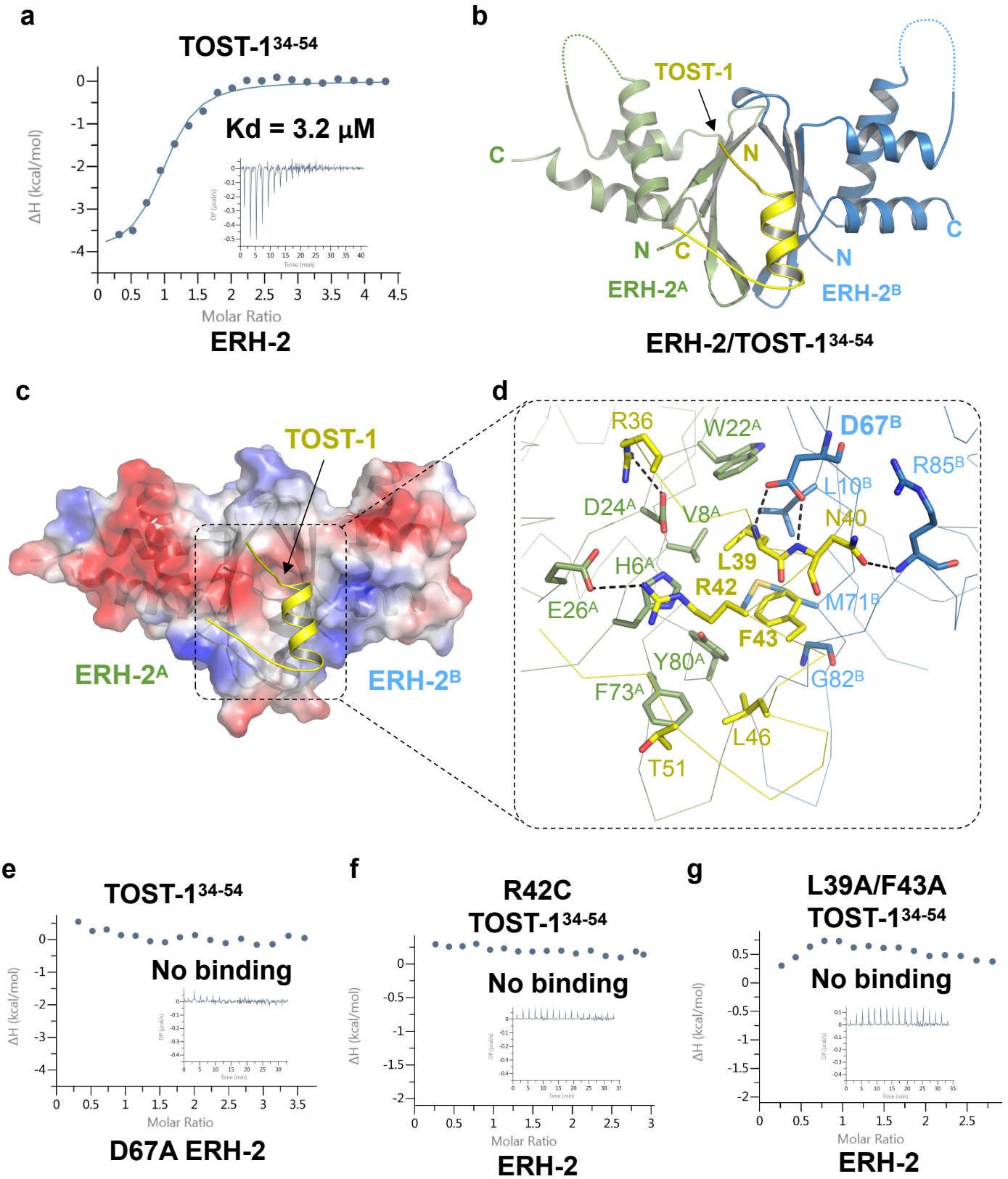
a
TOST-1^34-54
Kd = 3.2 µM
ΔH (kcal/mol)
Molar Ratio
ERH-2
b
TOST-1
C
N
N
C
N
C
ERH-2^A
ERH-2^B
ERH-2/TOST-1^34-54
c
TOST-1
ERH-2^A
ERH-2^B
d
R36
W22^A
D67^B
R85^B
L10^B
D24^A
V8^A
N40
H6^A
L39
R42
E26^A
M71^B
F43
Y80^A
G82^B
F73^A
L46
T51
e
TOST-1^34-54
No binding
ΔH (kcal/mol)
Molar Ratio
D67A ERH-2
f
R42C
TOST-1^34-54
No binding
ΔH (kcal/mol)
Molar Ratio
ERH-2
g
L39A/F43A
TOST-1^34-54
No binding
ΔH (kcal/mol)
Molar Ratio
ERH-2

Figure 4

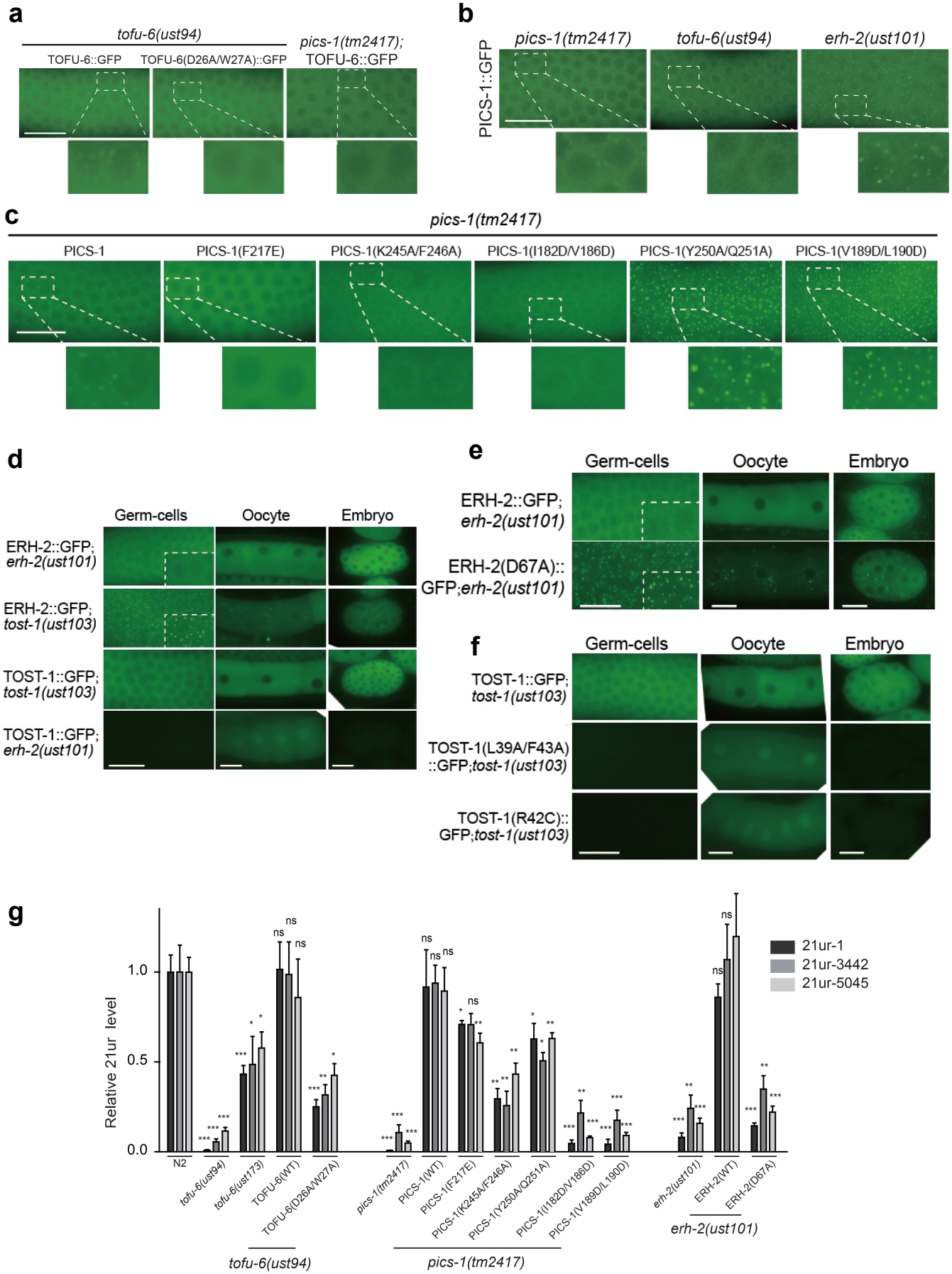
a
tofu-6(ust94)
TOFU-6::GFP
TOFU-6(D26A/W27A)::GFP
pics-1(tm2417);
TOFU-6::GFP
b
PICS-1::GFP
pics-1(tm2417)
tofu-6(ust94)
erh-2(ust101)
c
pics-1(tm2417)
PICS-1
PICS-1(F217E)
PICS-1(K245A/F246A)
PICS-1(I182D/V186D)
PICS-1(Y250A/Q251A)
PICS-1(V189D/L190D)
d
Germ-cells
Oocyte
Embryo
ERH-2::GFP;
erh-2(ust101)
ERH-2::GFP;
tost-1(ust103)
TOST-1::GFP;
tost-1(ust103)
TOST-1::GFP;
erh-2(ust101)
e
Germ-cells
Oocyte
Embryo
ERH-2::GFP;
erh-2(ust101)
ERH-2(D67A)::
GFP;erh-2(ust101)
f
Germ-cells
Oocyte
Embryo
TOST-1::GFP;
tost-1(ust103)
TOST-1(L39A/F43A)
::GFP;tost-1(ust103)
TOST-1(R42C)::
GFP;tost-1(ust103)
g
Relative 21ur level
1.0
0.5
0.0
21ur-1
21ur-3442
21ur-5045
N2
tofu-6(ust94)
tofu-6(ust173)
TOFU-6(WT)
TOFU-6(D26A/W27A)
pics-1(tm2417)
PICS-1(WT)
PICS-1(F217E)
PICS-1(K245A/F246A)
PICS-1(Y250A/Q251A)
PICS-1(I182D/V186D)
PICS-1(V189D/L190D)
erh-2(ust101)
ERH-2(WT)
ERH-2(D67A)
tofu-6(ust94)
pics-1(tm2417)
erh-2(ust101)

Figure 5

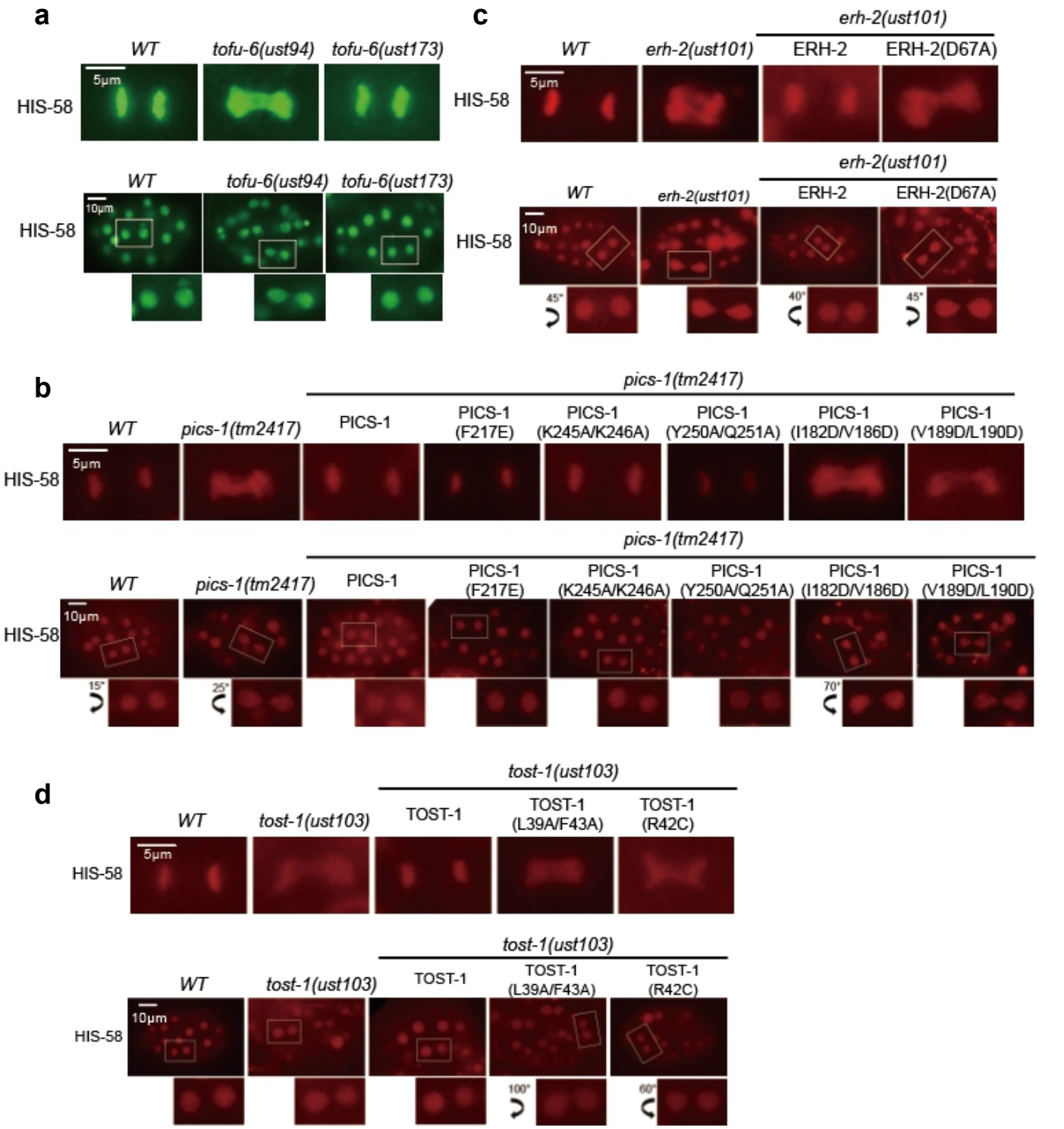
a
WT
tofu-6(ust94)
tofu-6(ust173)
HIS-58
5μm
10μm
c
erh-2(ust101)
WT
erh-2(ust101)
ERH-2
ERH-2(D67A)
HIS-58
5μm
10μm
45°
40°
b
pics-1(tm2417)
WT
pics-1(tm2417)
PICS-1
PICS-1 (F217E)
PICS-1 (K245A/K246A)
PICS-1 (Y250A/Q251A)
PICS-1 (I182D/V186D)
PICS-1 (V189D/L190D)
HIS-58
5μm
10μm
15°
25°
70°
d
tost-1(ust103)
WT
tost-1(ust103)
TOST-1
TOST-1 (L39A/F43A)
TOST-1 (R42C)
HIS-58
5μm
10μm
100°
60°

Figure 6